Mechanical Systems and Signal Processing 163 (2022) 108187

Contents lists available at ScienceDirect

Mechanical Systems and Signal Processing

journal homepage: www.elsevier.com/locate/ymssp

Novel regenerative braking method for transient torsional oscillation suppression of planetary-gear electrical powertrain

Feng Wang [a,b], Peng Ye [a], Xing Xu [a,*], Yingfeng Cai [a], Shaoyong Ni [c], Hongbo Que [d]

[a] Automotive Engineering Research Institute, Jiangsu University, Zhenjiang 212013, China
[b] State Key Laboratory of Engines, Tianjin University, Tianjin 300072, China
[c] Chery New Energy Automobile Co., Ltd., Wuhu 241009, China
[d] CRCC Qishuyan Institute Co., Ltd., Changzhou 213011, China

ARTICLE INFO

Keywords:
Torsional oscillation suppression
Angle-varying mesh stiffness
Planetary-gear powertrain
Backlash
Torsional oscillation-considered regenerative braking method

ABSTRACT

Electric regenerative braking systems have drawn much attention in the trends of energy-saving and emission-reduction requirements for electric vehicles. However, the significant differences between regenerative braking transmission chains and the traditional ones have lead to increasing oscillation and noise of electrical powertrain. With the application of planetary-gear transmission chains, adopting an advanced regenerative braking method becomes practical. This paper develops a novel regenerative braking method for transient torsional oscillation suppression of planetary-gear electrical powertrain (PGEP), which uses an angle-varying mesh stiffness-considered transmission model and a genetic algorithm-based method for allocation of electric regenerative braking torque. Simulations are conducted with various angle-varying mesh stiffness and backlash to compare the transient torsional oscillation-suppression performance of PGEP during regenerative braking transition process. For an initial speed of 80 km/h, simulation results show that the proposed torsional oscillation-considered electric regenerative braking torque allocating method performs the best comparing with the traditional methods, which has a 55% reduction in vehicle jerk and 36% improvement in torsional oscillation of PGEP. The AVL experiment results also demonstrated that torsional oscillation-considered regenerative braking method has considerable benefits in both transient torsional oscillation suppression of PGEP as well as enhancement of driving comfort.

1. Introduction

With the exacerbating problems of over-consumption on fossil energy and serious air pollution, new types of hybrid electric vehicles (HEVs) and pure electric vehicles (EVs) have attracted worldwide attention [1–4]. Meanwhile, energy-saving technologies of EVs and HEVs are being popularized in both academy and automotive industry, including electrical regenerative braking, advanced energy management strategy, logical mode transition control, and so on [5–8]. Detailed investigation results in [9] reveal that about 25% of energy is dissipated in form of the heat during the process of vehicle deceleration, regenerative braking is an effective way to recover braking energy loss of electric vehicles, especially for urban driving condition. Therefore, scholars world-widely have carried out comprehensive and in-depth research on regenerative braking system from various aspects.

* Corresponding author.
E-mail addresses: xuxing@ujs.edu.cn, bewater@ujs.edu.cn (X. Xu).

https://doi.org/10.1016/j.ymssp.2021.108187
Received 10 December 2020; Received in revised form 1 June 2021; Accepted 22 June 2021
Available online 29 June 2021

Most of traditional regenerative braking systems mainly focus on reducing fuel consumption [10] and enhancing hybrid braking safety, which require a closely combination of hydraulic braking and electric braking. Aimed at increasing energy recovery without wheel lockup, Ko et al. [11] presented a cooperative control algorithm for regenerative braking to arrange the regenerative braking force at front wheel and frictional braking force at rear wheel. Zhao et al. [12] proposed a power distribution strategy to achieve a comprehensive efficiency optimum to maximize the energy recovery and utilization efficiency considering the charge–discharge loss of ultracapacitor and battery as well as DC/DC converter loss. Zhang et al. [13] presented a dynamic braking torque distribution algorithm for the front and rear axle considering the influence of different slopes on regenerative braking recovery efficiency and safety. Pei et al. [14] integrated the recognition of braking intention from driver into the weight coefficient to achieve a dynamic distribution between hydraulic and regenerative braking torques. Li et al. [15] designed the dynamic coefficient used in pontryagin's minimum principle to recovery kinetic energy while braking for fuel cell hybrid locomotive, and then obtained an optimized braking speed curve which has maximum brake recovery rate. Qiu et al. [16] discussed two evaluating indicators of contribution brought by regenerative braking on electric vehicle's energy efficiency improvement of EV, namely the contribution ratio to the improvement of regenerative braking energy transfer efficiency and the contribution ratio to regenerative driving range. And the corresponding vehicle road tests were carried out under China typical city regenerative driving cycle. Li et al. [17] put forward a downshifting hierarchical control strategy during regenerative braking to ensure braking safety and energy efficiency during the process of downshift.

However, with respect to conventional vehicles, the ride comfort issue for PGEP-based EVs in the process of regenerative braking requires special consideration, as the reverse transmitting direction of powertrain energy. It is a special mode transition process for electric vehicles transmitting from motor-driven mode to regenerative braking mode while deceleration [18]. Zhang et al. [19] proposed a novel control method for permanent magnet synchronous motor (PMSM) considering the transmission influence on the high-dynamic anti-lock braking process of pure electric vehicle, the results show that the mode-switching PMSM control can effectively compensate for transmission effects and significantly improve the comfort and stability during anti-lock braking of EV. To suppress the significant torque interruption during the regenerative braking both in up-shift and down-shift process, Paul et al. [20] proposed a power-on shifting control strategy for regenerative braking as well as an energy-safety oriented braking strategy. The improvements of efficiency and recovery capability are verified through a typical deceleration driving cycle and a specially designed daily deceleration scenario. Zhang et al. [21] presented the time-varying delays compensation algorithm for electrified powertrain to reduce or eliminate negative effect upon the performance of cooperative control for regenerative and hydraulic braking based on a predictive scheme. Taken into consideration the effects of the powertrain backlash and flexibility on vehicle drivability during regenerative deceleration, Lv et al. [22–23] developed a mode-switching-based active control algorithm with a hierarchical architecture and aimed at providing compensation for powertrain backlash and flexibility, the result shows that the torsional vibration during regenerative braking is obviously suppressed. Zhao et al. [24] investigated the downshifting model of HEVs with dual clutch transmission, effectively reduced the workload of hydraulic mechanical braking system and elevated the recovery braking energy. All the studies above show that the introduction of coordination control reduces the torque fluctuation during the mode-switch process and improves the vehicle drivability. Although outstanding progress has been made on development and refinement of algorithms to enhance the driving comfort during the process of regenerative braking, most regenerative braking models assume that the components of transmission operate under a rigid contact condition, ignoring the angle-varying mesh stiffness and backlash of planetary-gear powertrain.

With the increasing demand for drivability and low vibration of EVs powertrain, it is worth considering comprehensive effects so that teeth backlashes, angle-varying mesh stiffness, and regenerative electric braking torque fluctuation can be observed simultaneously. Thus, a more accurate transmission system model is essential to be considered in the process of energy recovery. An EV equipped with planetary-gear powertrain is taken into account in this paper, and the problem of suppressing transient torsional oscillation is converted into finding the optimal distribution coefficients of regenerative braking torque by genetic algorithm. The contributions of the proposed regenerative braking method lie in the following three aspects:

- The effective of angle-varying mesh stiffness and backlash of planetary gear pair on torsional oscillation during the transition from motor-driven mode (MD) to regenerative braking mode (RB) are taken into consideration to build the powertrain model.
- A novel method for distributing the regenerative braking torque and suppressing the transient torsional oscillation of planetary-gear electric powertrain is proposed.
- The problem of suppressing transient torsional oscillation is converted into solving the optimal distribution coefficients of regenerative braking torque by genetic algorithm.

Thusly, this paper comes up with a novel regenerative braking method to suppress transient torsional oscillation of planetary-gear electrical powertrain during the transition process of MD-to-RB. The smooth performance of planetary-gear electrical powertrain will be improved significantly when adopting this method comparing with the traditional ways. The remaining of this paper is organized as follows: In Section 2, the structure of planetary-gear electrical powertrain and transient torsional oscillation model related to regenerative braking are introduced, considering angle-varying mesh stiffness and backlash of planetary gear pair. In Section 3, torsional oscillation-considered regenerating braking method is performed to cope with the optimization targets of both low torsional oscillation in planetary-gear electrical powertrain and a high ride comfort of EVs. An AVL test platform is built to verify the effectiveness of torsional oscillation-considered regenerative braking method in Section 4. At last, conclusions and outlines for the future research are given in Section 5.

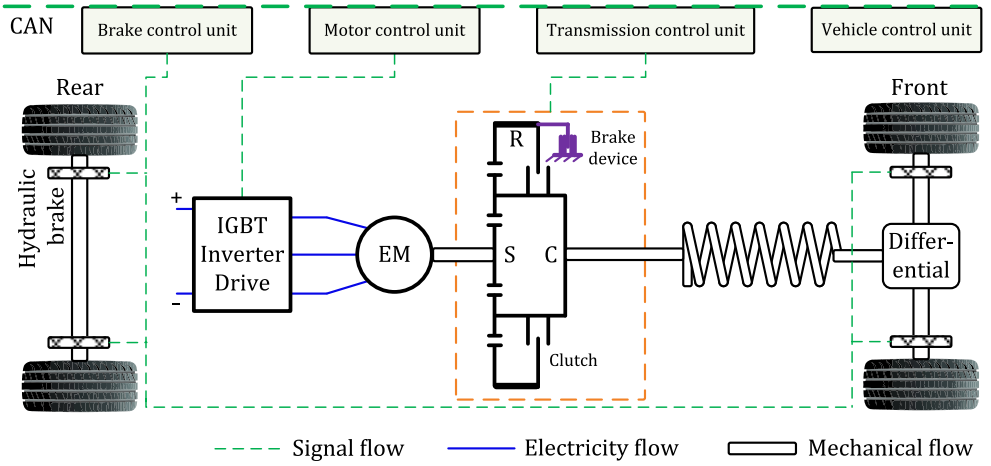

Fig. 1. Schematic graph of planetary-gear electrical powertrain equipped in EV.

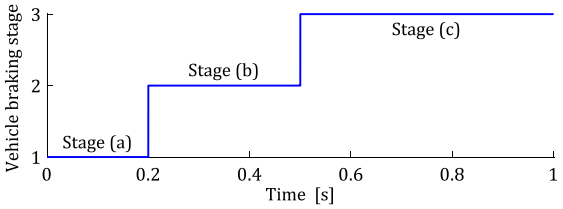

Fig. 2. Stage division of vehicle braking process.

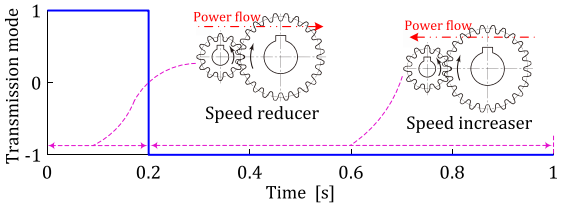

Fig. 3. Transmission mode during MD-to-RB process.

2. Powertrain transient torsional oscillation model and analysis

2.1. Planetary-gear electrical powertrain configuration

The planetary-gear electrical powertrain in this case can be classified as a series EV system, and its configuration is shown in Fig. 1. This powertrain is mainly comprised of an electric motor, the proposed PGEP, wheels and the vehicle frame which are connected together via spring-damper torsional shafts. The drive wheels are driven by permanent magnet synchronous motor (PMSM) with a two-speed planetary gear set, whose working mode depends on the states of clutch and brake device. The traction motor is connected to sun gear and the final drive is linked to carrier. There is also a hydraulic brake attached to each of half-drive-shaft for traditional braking.

The architecture of system signal flow is as follows: The vehicle control unit (VCU) is used to analyze the driver inputs and control the motor control unit (MCU), transmission control unit (TCU) and braking system (including motor regenerative braking and hydraulic frictional braking). All of these control units communicate through a CAN 2.0 network, and the mode transition of electrical powertrain relies on the states of dry clutch, brake device and electric motor [25–28].

2.2. Regenerative braking process description

During the whole MD-to-RB process studied in this paper, the clutch is disengaged and the brake device is kept combined. The regenerating braking starts with a stage when clutch open, and the traction motor controls the vehicle at a constant speed. When the brake pedal is pressed down and the power battery is in a rechargeable state, mode transition from MD to RB comes into operation. As

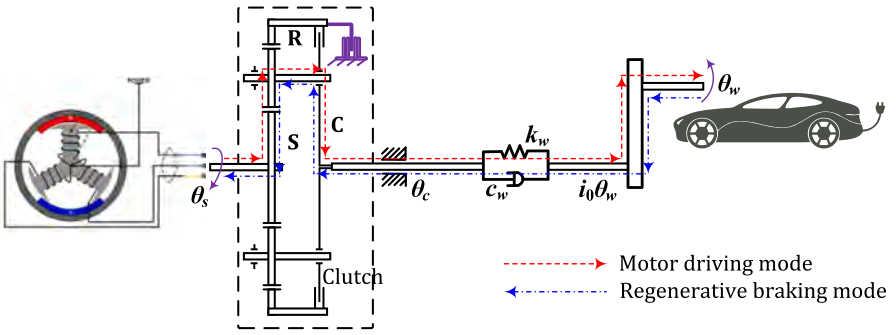

Fig. 4. Schematic model of planetary-gear electrical powertrain.

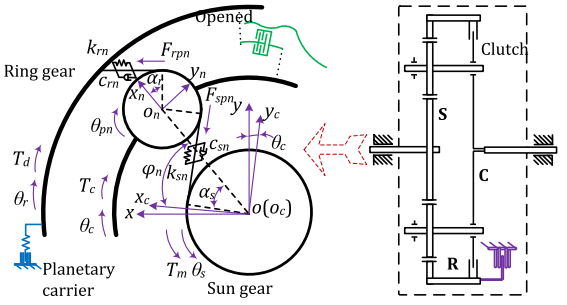

Fig. 5. Dynamic torsional model of epicyclic gear.

demonstrated in Fig. 2, the mode transition process consists of three phases: (a) the motor-driven stage, (b) the braking torque establishing stage, (c) the regenerative braking stage.

(a). In the first stage, electric motor provides vehicle driving torque and works in motor-driven mode. (b). In the second stage, the braking torque is provided by electric motor and hydraulic brake system, and the establishing process lasts about 0.3 s. (c). In the final stage of mode transition, braking deceleration/torque keeps a constant value. It is of great significance that a detailed planetary-gear electrical powertrain needs to be considered since the transmission state of the vehicle has changed from speed-decrease transmission to speed-increase transmission during the MD-to-RB process (shown as Fig. 3).

2.3. Transient torsional oscillation model of PGEP during the regenerative braking transition process

A fully EV powertrain model with electric motor, planetary gear and shaft is considered during the regenerative braking transition process, Fig. 4 shows a conceptual sketch of power flow in planetary-gear electrical powertrain [29,30]. The path of power is motor-to-wheel in motor driving mode and wheel-to-motor in regenerative braking mode. There are four main components, including motor, epicyclic gear, drive shaft and vehicle body, thusly several freedoms of motion are taken into consideration as shown in Fig. 4 and Fig. 5. Three coordinate systems are defined in order to analyze the torsional kinematic characteristics expediently, namely the stationary reference frame *oxy*, the rotary reference frame $o_cx_cy_c$, and the synchronization reference frame $o_nx_ny_n$ (n = 1,…,*N*).

Concerning the effect of power trains on MD-to-RB transition process, dynamic torsional of PGEP is finally modelled using torsional lumped parameters, considering angle-varying mesh stiffness and backlash of the planetary gear pair. Since this study mainly focus on the suppression of transient torsional oscillation in planetary-gear electrical powertrain, some assumptions are given to enhance the computational efficiency. For instance: road slope is zero; vehicle runs only longitudinally; the final drive and differential exert equal torques on the half shafts with no tire slippage; both support bearings and tires are considered to be inelastic.

Based on the above-mentioned assumptions, a simplified dynamical spring-damper model with 4 + N (N is the number of planet gears) degree of freedom in planetary-gear electrical powertrain is derived via Newtonian method to investigate the transmission mechanism as Eqs. (1-7), the lateral vibration, the transmission error and tooth modification are not considered. Clockwise direction is defined as the positive direction, while the counter-clockwise direction is defined as the negative direction.

$$J_s \cdot \left(\ddot{\theta}_s + \ddot{\theta}_c\right) = T_m + \sum_{n=1}^{N}\left(r_{bs}F_{spn}\right) \tag{1}$$

$$J_r \cdot \left(\ddot{\theta}_r + \ddot{\theta}_c\right) = \sum_{n=1}^{N}\left(r_{br}F_{rpn}\right) + k_{B1} \cdot \left(\theta_r + \theta_c\right) \tag{2}$$

$$\left(J_c + Nm_p r_c^2\right)\cdot\ddot{\theta}_c = \left[c_w\cdot\left(\dot{\theta}_c - i_0\dot{\theta}_w\right) + k_w\cdot\left(\theta_c - i_0\theta_w\right)\right] - \sum_{n=1}^{N}\left[r_c\cdot\left(F_{spn}cos\alpha_s + F_{rpn}cos\alpha_r\right)\right] \tag{3}$$

$$J_{pn}\ddot{\theta}_{pn} = r_{bp}\cdot\left(F_{spn} + F_{rpn}\right) \tag{4}$$

$$\left(\delta m r_w^2\right)\cdot\ddot{\theta}_w - i_0\cdot\left[c_w\cdot\left(\dot{\theta}_c - i_0\dot{\theta}_w\right) + k_w\cdot\left(\theta_c - i_0\theta_w\right)\right] = -T_d \tag{5}$$

$$F_{spn} = cos\beta\cdot\left\{k_{sn}\cdot\kappa\left(r_{bs}\theta_s - r_{bp}\theta_{pn}\right)\cdot cos\beta\right\} + cos\beta\cdot\left\{c_{sn}\cdot\left(r_{bs}\dot{\theta}_s - r_{bp}\dot{\theta}_{pn}\right)\cdot cos\beta\right\} \tag{6}$$

$$F_{rpn} = cos\beta\cdot\left\{k_{rn}\cdot\kappa\left(r_{br}\theta_r + r_{bp}\theta_{pn}\right)\cdot cos\beta\right\} + cos\beta\cdot\left\{c_{rn}\cdot\left(r_{br}\dot{\theta}_r + r_{bp}\dot{\theta}_{pn}\right)\cdot cos\beta\right\} \tag{7}$$

where θ_s, θ_r, θ_{pn}, θ_c and θ_w denote the dynamic angular displacements of sun gear, ring gear, planet gears, output carrier and wheel, and their corresponding first-order and second-order derivatives represent angular velocity and angular acceleration; J_s, J_r, J_{pn}, J_c and m_p denote the inertia of sun gear, ring gear, planetary gear, planetary carrier and the mass of planetary gear, respectively; r_{bs}, r_{br}, r_{bp} and r_c represent the pitch radius of sun gear, ring gear, planetary gear and the length between center of a planetary gear and the planetary carrier, respectively; k_w and c_w denote the equivalent torsional stiffness and damping constant of flexible output shaft, respectively; β denotes the helix angle of helical gear; m and δ denote the vehicle mass and its equivalent revolving mass coefficient, thusly $(\delta m r_w^2)$ indicates the effective inertia of the vehicle, drive shafts and wheels; i_0 denotes the final drive ratio; r_w denotes the radius of wheels; k_{B1} denotes the equivalent stiffness of wedge brake device; α_s, α_r denote the pressure angles of sun gear and ring gear, respectively; T_m denotes the driving torque or regenerative braking torque of electric motor imposed on input shaft; T_d represents external retarding torques including vehicle driving resistance torque and hydraulic braking torque.

Angle-varying mesh stiffness k_{sn} and k_{rn} are calculated as Eq. (8-9), detailed calculation methods based on loaded tooth contact analysis (LTCA) can be seen in reference [31,32]; c_{sn}, c_{rn} denote the equivalent mesh damping constants of sun-planet gear pair and ring-planet gear pair, which are proposed in Eq. (10); the included angle φ_n is shown as Eq. (11).

$$k_{sn}(\theta_s) = a_0 + \sum_j\left\{a_j cos\left[jz_s\cdot\left(\theta_s - \varphi_n\right)\right]\right\} + \sum_j\left\{b_j sin\left[jz_s\cdot\left(\theta_s - \varphi_n\right)\right]\right\} \tag{8}$$

$$\begin{aligned} k_{rn}(\theta_r) = a_0 &+ \sum_j\left\{a_j cos\left[jz_r\cdot\left(\theta_r - \varphi_n - \frac{\pi}{z_r}\cdot\ mod\ \left(z_p, 2\right)\right)\right]\right\} \\ &+ \sum_j\left\{b_j sin\left[jz_r\cdot\left(\theta_r - \varphi_n - \frac{\pi}{z_r}\cdot\ mod\ \left(z_p, 2\right)\right)\right]\right\} \end{aligned} \tag{9}$$

$$c_{\tau n} = 2\xi\sqrt{\frac{k_{\tau n0}J_\tau J_{pn}}{J_\tau r_{b\tau}^2 + J_{pn}r_{bp}^2}} \cdots\cdots \tau = s, r \tag{10}$$

$$\varphi_n = 2\pi\frac{(n-1)}{N} \tag{11}$$

where z_s, z_r and z_p represent the teeth number of sun, ring and planet gears, respectively; a_0, a_j and b_j represent the j-th Fourier expanding coefficients for angle-varying meshing stiffness. And 'mod' denotes the remainder function, which indicates the remainder value divided by '2' in Eq. (9).

The normal-clearance functions of sun-planet and ring-planet gear pairs are shown as Eqs. (12-13).

$$\kappa\left(r_{bs}\theta_s - r_{bp}\theta_{pn}\right) = \begin{cases} \left(r_{bs}\theta_s - r_{bp}\theta_{pn}\right) - \Delta b_{sn} & \left(r_{bs}\theta_s - r_{bp}\theta_{pn}\right) > \Delta b_{sn} \\ 0 & -\Delta b_{sn} \leqslant \left(r_{bs}\theta_s - r_{bp}\theta_{pn}\right) < \Delta b_{sn} \\ \left(r_{bs}\theta_s - r_{bp}\theta_{pn}\right) + \Delta b_{sn} & \left(r_{bs}\theta_s - r_{bp}\theta_{pn}\right) < -\Delta b_{sn} \end{cases} \tag{12}$$

$$\kappa\left(r_{br}\theta_r + r_{bp}\theta_{pn}\right) = \begin{cases} \left(r_{br}\theta_r + r_{bp}\theta_{pn}\right) - \Delta b_{sn} & \left(r_{br}\theta_r + r_{bp}\theta_{pn}\right) > \Delta b_{rn} \\ 0 & -\Delta b_{rn} \leqslant \left(r_{br}\theta_r + r_{bp}\theta_{pn}\right) < \Delta b_{rn} \\ \left(r_{br}\theta_r + r_{bp}\theta_{pn}\right) + \Delta b_{sn} & \left(r_{br}\theta_r + r_{bp}\theta_{pn}\right) < -\Delta b_{rn} \end{cases} \tag{13}$$

where Δb_{sn}, Δb_{rn} represent the 1/2 backlashes of the sun-planetary and ring-planetary gear pairs, respectively.

2.4. Longitudinal vehicle dynamic model

In the planetary-transmission longitudinal EV dynamic model, the tractive force needs to overcome various resistances to keep the force balance in motor-driven mode, which consist of wheel rolling resistance, aerodynamic drag force, and acceleration resistance

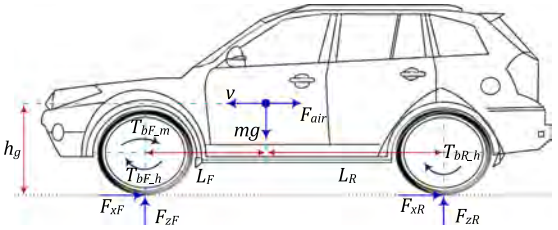

Fig. 6. Schematic graph of front-drive longitudinal EV dynamic model.

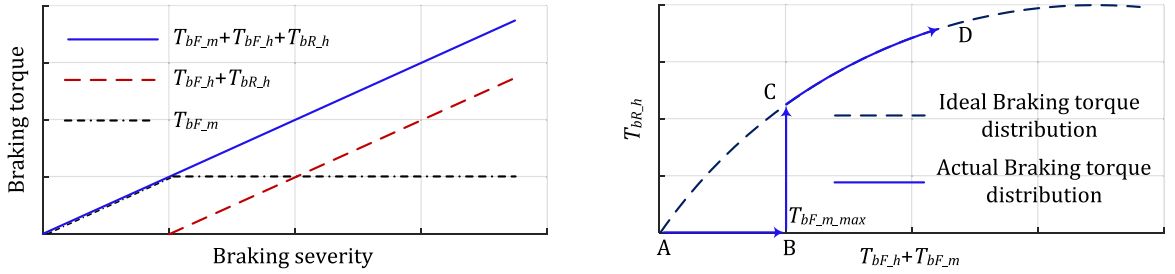

(a) Braking torque distribution between electric motor and hydraulic braking system;

(b) Braking torque distribution between front and rear wheel.

Fig. 7. Schematic diagram of braking torque for front-drive EV.

[33], while reaching the requirement of braking acceleration in regenerative braking mode which includes the utilization of adhesion coefficient and braking stability simultaneously.

When the EV works in motor-driven mode, driving torque that the electric motor imposed on input shaft and external retarding torque imposed on output shaft can be calculated as Eq. (14).

$$\begin{cases} T_m = \dfrac{r_w}{i_0(i+1)} \cdot \left(mgf_r + \dfrac{C_D A}{21.15} v^2(t) + \delta m \cdot a(t) \right) \\ T_d = r_w \cdot \left(mgf_r + \dfrac{C_D A}{21.15} v^2(t) \right) \end{cases} \tag{14}$$

where i represents the reduction ratio as z_r/z_s; f_r and C_D denote the rolling friction coefficient and airflow coefficient, respectively; A indicates the effective vehicle frontal area; $v(t)$ and $a(t)$ denote the current longitudinal velocity and acceleration of the vehicle, respectively.

As the driver's intention to brake is identified based on fuzzy logic, the front-drive EV changes to regenerative braking mode (shown in Fig. 3), the relevant longitudinal forces on the vehicle are shown in Fig. 6. Considering the influence of longitudinal mass transfer during the course of braking, the vertical forces of front wheel and rear wheel are calculated as Eq. (15).

$$F_{zF} = \frac{m(gL_R + zgh_g)}{2(L_F + L_R)}; F_{zR} = \frac{m(gL_F - zgh_g)}{2(L_F + L_R)} \tag{15}$$

where L_F and L_R represent the distance from gravity center to front and rear wheel; g denotes gravity acceleration; z represents the braking severity, which is related to the driver's braking intention and vehicle state parameters; h_g denotes height of vehicle gravity center; F_{xF} and F_{xR} represent longitudinal tire forces of the front and rear wheels; T_{bF_h} and T_{bF_m} represent the braking torques on front wheels provided by hydraulic brake system and electric motor, and the braking torque of rear wheels T_{bR_h} is completely provided by traditional hydraulic brake system owing to the front-driven structure in this study.

To achieve a maximum utilization of adhesion coefficient and optimum braking stability, the ideal curve of braking force distribution is designed to prevent wheel lockup on both front and rear wheel, which is expressed as Eq. (16) [34,35].

$$\begin{cases} F_{xR} = \dfrac{mg}{2h_g} \cdot \sqrt{L_R^2 + \dfrac{4h_g \cdot (L_F + L_R)}{mg} F_{xF}} - \dfrac{mgL_R}{2h_g} - F_{xF} \\ F_{xF} + F_{xR} = zmg \leqslant \varphi \cdot (F_{zF} + F_{zR}) \end{cases} \tag{16}$$

where φ is the road adhesion coefficient.

Because only the front wheels can provide regenerative braking torque for front-drive EVs, a traditional ideal curve of braking force distribution can not ensure a highest regeneration energy recovery [36,37]. The area above the ideal distribution curve in Fig. 7(b)

Table 1
Key parameters of the front-drive EV equipped with planetary-gear set.

Components	Description
PGEP driveline	Normal module: 2 mm; Spiral angle: 15.5° Teeth number: Sun gear: 61; Planet gear: 25; Ring gear: 111 Tooth width: 45 mm; Number of planet gears: 4 Ratio of main reducer: 4.3 Torsional stiffness of brake device B1: 5.5×10^5 Nm/rad Torsional stiffness of flexible output shaft: 6.0×10^5 Nm/rad Torsional damping of flexible output shaft: 210 Nms/rad
Electric motor	Type: permanent magnet synchronous motor (PMSM) Maximum power: 80 kW; Maximum speed: 7200 rpm Peak torque: 250 N·m (motor); −180 N·m (generator)
Battery pack	Type: NiMH Nominal voltage: 387 V Capacity: 60 kW·h
Vehicle	Vehicle mass: 1430 kg Frontal area of vehicle: 1.56 m^2; Aerodynamic drag: 0.30 Tire rolling resistance coefficient: 0.0165 Drive wheel radius: 0.289 m Gravity center height: 0.6 *m*

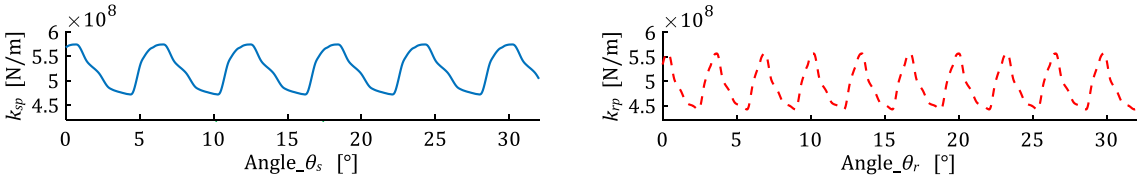

(a) Mesh stiffness of planet-sun gear; (b) Mesh stiffness of planet-ring gear.

Fig. 8. Angle-varying mesh stiffness of planetary-gear transmission.

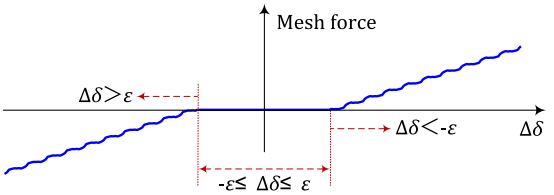

Fig. 9. Teeth mesh force containing backlash and fluctuation stiffness.

means that the rear wheel will lock before the front wheel, it is unstable and should be avoided as much as possible. In order to consider both the EV braking stability and the regeneration energy recovery, regenerating the braking energy in slight and medium degree of braking usually becomes the most concerned point. Hence, the strategy to distribute braking torque to electric motor and hydraulic braking system employed in this front-drive EV is shown as Fig. 7(a), where the braking torque is mainly provided by electric motor as much as possible and compensated by the hydraulic braking torque when the electric braking torque is insufficient. As consequence, the actual braking torque distribution between the front and rear wheel is not ideal but practical (ABCD in Fig. 7(b)), which takes account of braking stability and regeneration energy recovery, simultaneously.

On the basis of above analysis, driving torque of electric motor imposed on input shaft and external retarding torque excreted on output shaft in regenerative braking mode are eventually obtained by Eq. (17).

$$\begin{cases} T_m = -\dfrac{T_{bF\_m}}{i_0(i+1)} \\ T_d = r_w \cdot \left(mgf_r + \dfrac{C_D A}{21.15} v^2(t) \right) + T_{bF\_h} + T_{bR\_h} \end{cases} \tag{17}$$

2.5. Model solution and torsional oscillation analysis

In this section, model validation is performed by means of a simulation built in the environment of MATLAB/*Simulink* R2020a. The front-drive EV model proposed in this paper was set at a initial vehicle speed of 80 km/h, and the brake pedal was designed to increase

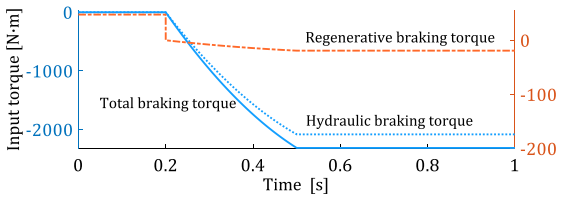

Fig. 10. Hydraulic braking-dominant braking torque distribution (Hd-BD).

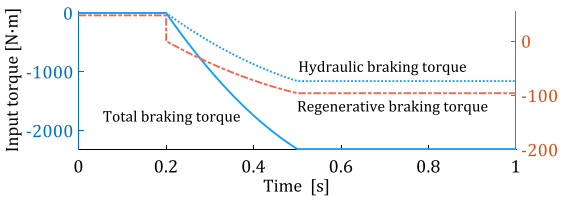

Fig. 11. Equalization braking torque distribution (Eq-BD).

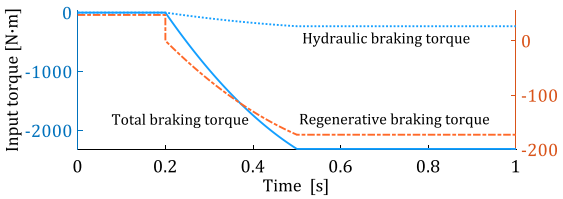

Fig. 12. Electric braking-dominant braking torque distribution (Ec-BD).

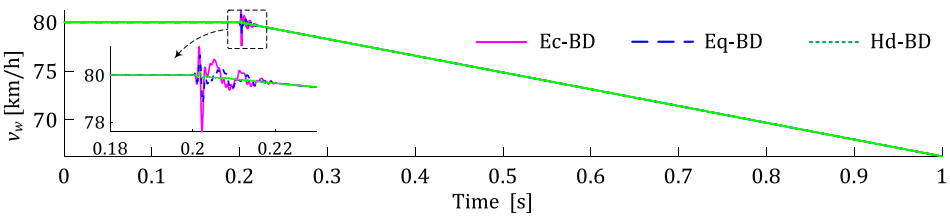

Fig. 13. Real-time vehicle speed with various braking torque distribution.

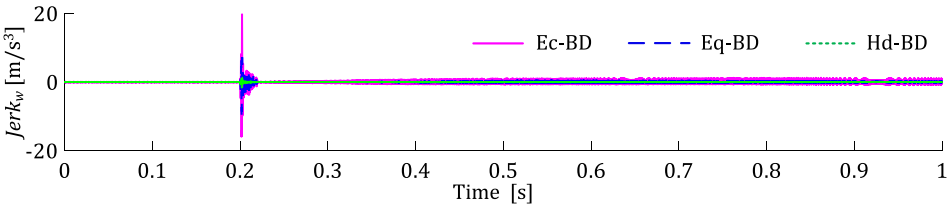

Fig. 14. Vehicle jerk with various braking torque distribution.

from 0 to 30% within about 0.3 s. The braking severity is approximate 0.35. The main parameters of the front-drive EV equipped with planetary-gear transmission for simulations are listed in Table 1.

Angular displacement-varying mesh stiffness of the planet-sun gear pair and planet-ring gear are illustrated as Fig. 8, it can be recognized that the fluctuation of mesh stiffness together with backlash of gear pair contribute to the dynamic meshing force in Fig. 9 [38,39].

When the opening of brake pedal is set to 30%, the maximum regenerative braking torque provided by electric motor meets the braking demand, three different distributing coefficients of brake torque (hydraulic braking-dominant braking torque distribution in Fig. 10, equalization braking torque distribution in Fig. 11 and electric braking-dominant braking torque distribution in Fig. 12) are

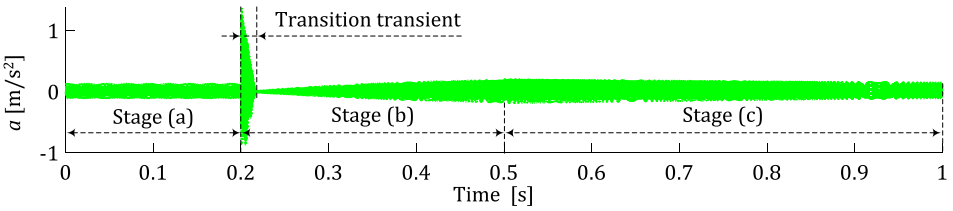

Fig. 15. a_{rp} during MD-to-RB transition process (Hd-BD).

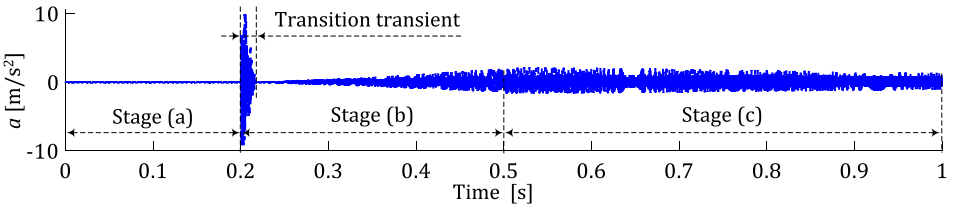

Fig. 16. a_{rp} during MD-to-RB transition process (Eq-BD).

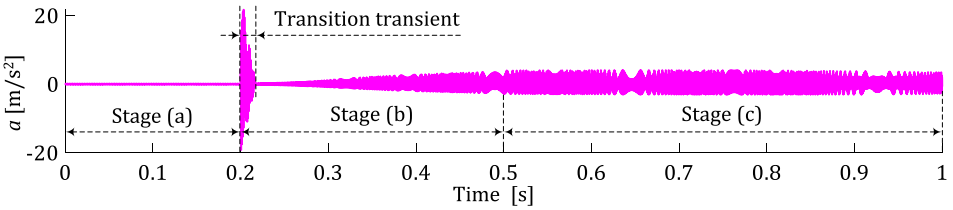

Fig. 17. a_{rp} during MD-to-RB transition process (Ec-BD).

put forward to analyze their effect on transient torsional oscillation of planetary-gear electrical powertrain during MD-to-RB transition.

In Fig. 13, the system is launched from a uniform velocity at 80 km/h and undergoes an regenerative braking at $t = 0.2$ s. Throughout this period, vehicle deceleration is realized by traction/generator motor and hydraulic braking system. The real-time vehicle speed in Fig. 13 demonstrates that the output of the mathematical model precisely follows the demanding speed. When the transmission direction of power flow changes, the gear pair will knock in the process of backlash elimination and further couple with angle-varying mesh stiffness, the inevitable fluctuation of longitudinal vehicle speed was occurred, and vehicle speed fluctuation (0.2 ~ 0.22 s) with Ec-BD is significantly higher than that of Eq-BD and Hd-BD, that is to say, the influence of electrical braking torque on ride comfort is greater than hydraulic braking torque, which is owing to the involvement of PGEP in the electrical braking mode. Similar trends are found in Fig. 14, vehicle jerk increases with the participation of regenerative braking, the maximum jerk value is more than 20 m/s^3 with Ec-BD.

In addition, excessive relative torsional oscillation between the ring and planet gear pairs of PGEP may lead to unexpected instability [40–43], which will possibly shorten the lifespan of PGEP, even cause fatal accidents during MD-to-RB mode transition process. Thusly, vibration acceleration a_{rp} is selected as the evaluation object and represented by Eq. (18).

$$a_{rp} = \frac{1}{N} \cdot \left\langle \sum_{n=1}^{N} \left[r_{bp} \ddot{\theta}_{pn} - r_{br} \cdot \left(\ddot{\theta}_r + \ddot{\theta}_c \right) \right] \right\rangle \tag{18}$$

The simulation results of a_{rp} during MD-to-RB transition process are shown in Fig. 15–17, torsional vibration reveals different characteristics corresponding to three working stages. In stage (a), the PGEP rotates at a constant speed and the external torques remain unchanged, a_{rp} represents a stable gear-mesh frequency variation which is mainly attributed to the excitation by angle-varying meshing stiffness. In stage (b), braking system including regenerative braking motor and hydraulic braking system start to work and the corresponding braking torque gradually increases. In consequence, a_{rp} behaves as a continuous increase in response to the growth of braking severity. In stage (c), the braking torque reaches the demanding and keeps stationary, torsional oscillation was restrained while the vehicle speed and rotational speed of PGEP continuous decreasing. Torsional oscillation during a transient transition process (0.2–0.22 s) should be set as high priority owing to its impact on the transition quality of MD-to-RB. It is noteworthy that the nonlinear response of a_{rp} is exhibited in Eq-BD and Ec-BD with the increased proportion of regenerative braking torque, conclusion is obtained that the proportion of electric braking torque directly affects the transient stability of the planetary-gear electrical powertrain.

As an important factor while affects the transition quality of MD-to-RB, transient kinematic analysis of the transmission with different teeth backlashes are studied in order to design a dynamical transmission system. Responses of real-time vehicle speed, vehicle

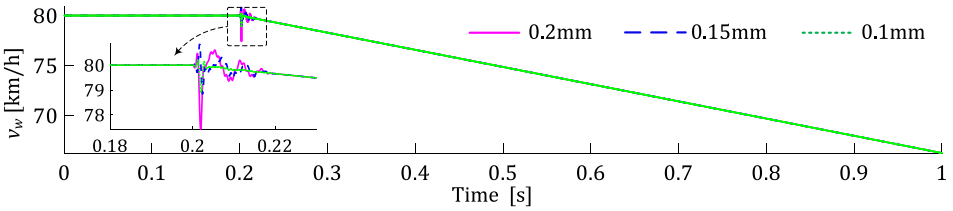

Fig. 18. Real-time vehicle speed with various backlashes.

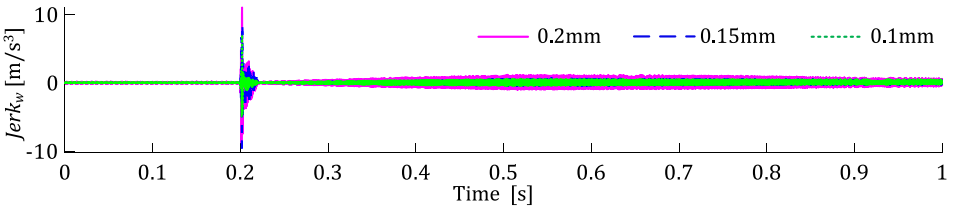

Fig. 19. Vehicle jerk with various backlashes.

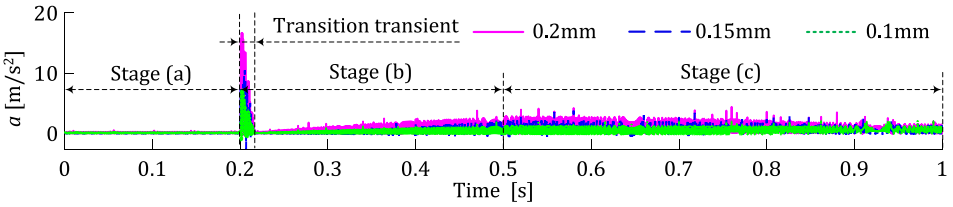

Fig. 20. Envelope of a_{rp} during MD-to-RB transition process with various backlashes.

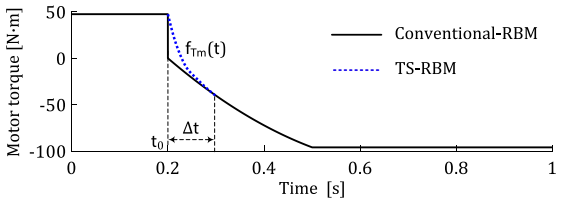

Fig. 21. Motor torque during MD-to-RB process.

jerk and the envelope of a_{rp} in Figs. 18–20 indicate that the increasing of backlash aggravates the torsional oscillation during the MD-to-RB process. Therefore, it is necessary to consider various factors such as lubrication requirement and drivability during regenerative braking when design the gear transmission system for electric vehicle.

3. Torsional oscillation-considered regenerating braking method of EVs

As described in more detailed in previous section, transient torsional oscillation and undesirable vehicle jerk during MD-to-RB process obviously affect the driving comfort and braking stability which is mainly attributed to the interaction between tooth backlash and the sudden change of motor torque. In conventional regenerative braking strategy, the electric braking torque decreases immediately from driving mode (positive torque) to generation mode (negative torque) owing to the motor torque can be applied instantaneously [44]. In the existing control strategies of regenerative braking system, braking safety and energy recovery efficiency are considered as the main core during regenerative braking process, however, the rapid change ratio of electric braking torque coupling with the internal excitations (backlash and angle-varying mesh stiffness) in the transmission system will obviously induce torsional vibration, and then affect the drive comfort in the process of regenerative braking. As shown in Fig. 21, the motor torque decreases immediately from 50 N·m to 0 N·m at 0.2 s in the case of conventional regenerative braking method (Conventional-RBM). A torsional oscillation-considered regenerating braking method (TS-RBM) for EVs is firstly proposed in this paper with a smooth curve $f_{Tm}(t)$ (shown as Eq. (19)) rather than the one abruptly rises or falls in Conventional-RBM. c_1, c_2, c_3, c_4 denote the curve coefficients of regenerating braking torque transition process, which can be optimized to achieve a lower torsional oscillation during the mode

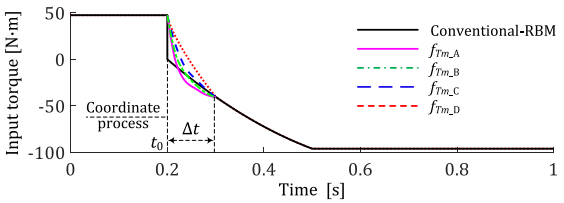

Fig. 22. Four types of motor torque during MD-to-RB process.

Table 2
Sensitivity analysis for vehicle jerk and torsional oscillation.

Conventional-RBM	TS-RBM	Jerk [m/s^3]	Change rate	RMS [m/s^2]	Change rate
Jerk: 10.1 m/s^3	f_{Tm_A}	8.0	15%	5.0	10%
	f_{Tm_B}	7.3	32%	4.6	18%
RMS: 5.6 m/s^2	f_{Tm_C}	4.9	51%	4.2	25%
	f_{Tm_D}	6.0	44%	4.4	22%
Sum of changing rate	○	○	1.42 Norm: 0.65	○	0.75 Norm: 0.35

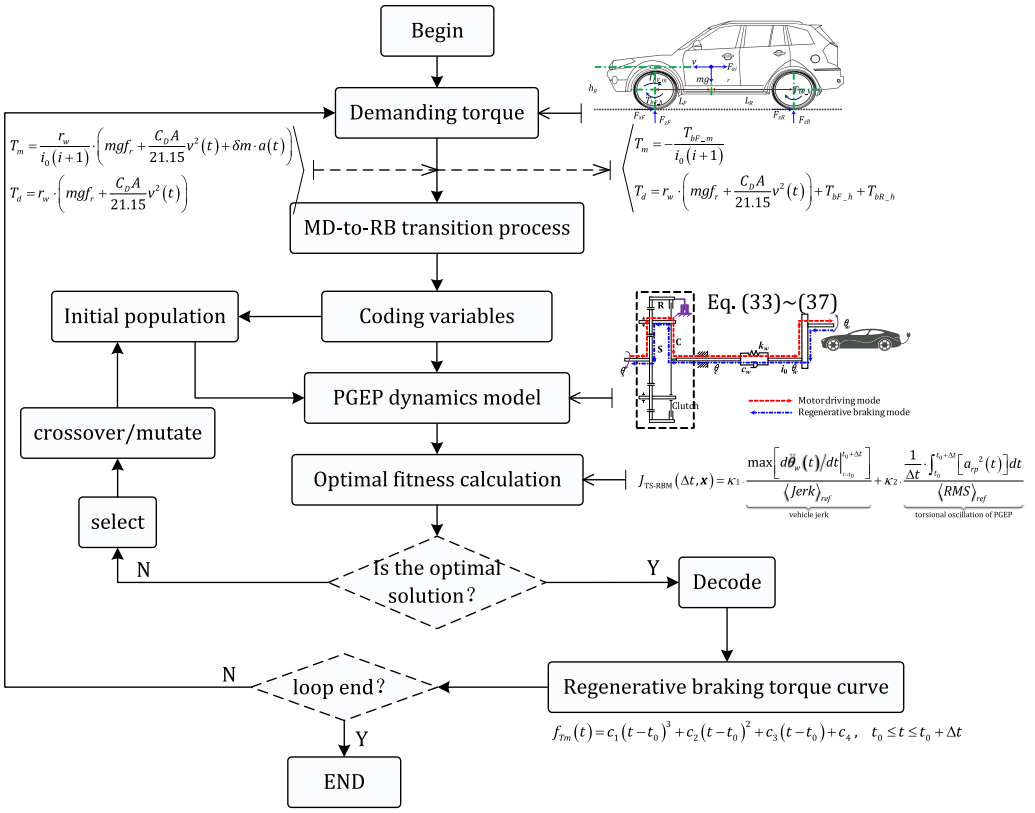

Fig. 23. Detailed optimization process of genetic algorithm for TS-RBM.

transition.

$$f_{Tm}(t) = c_1(t-t_0)^3 + c_2(t-t_0)^2 + c_3(t-t_0) + c_4, \quad t_0 \leqslant t \leqslant t_0 + \Delta t \tag{19}$$

The traditional index to elevated the vehicle longitudinal comfort is only the vehicle jerk, however, the noise of PGEP when running at high rotational speed is rather high. Thusly, combining the objective of suppression of torsional oscillation, TS-RBM can be regarded as a constrained multi-objective optimization problem including vehicle jerk of EV and torsional oscillation of PGEP simultaneously.

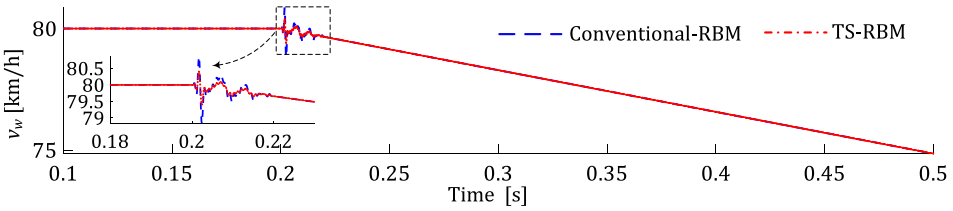

Fig. 24. Dynamic vehicle speed in Conventional-RBM and TS-RBM (simulation).

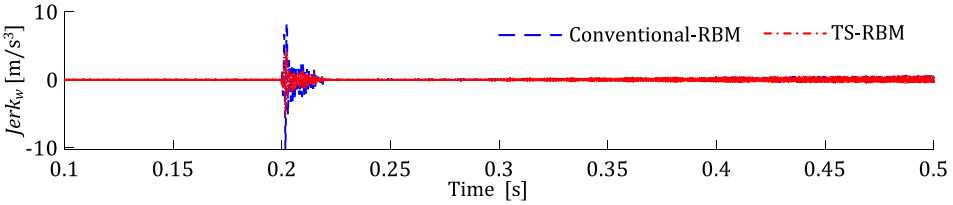

Fig. 25. Vehicle jerk responses of EVs in Conventional-RBM and TS-RBM (simulation).

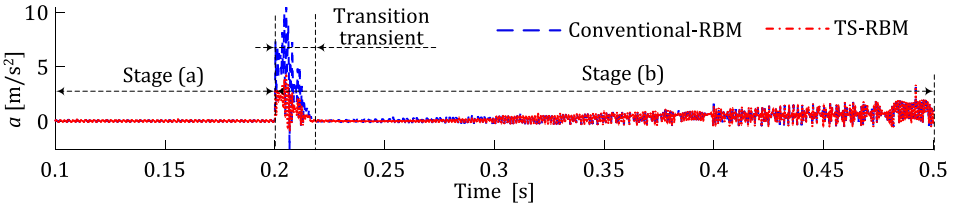

Fig. 26. Envelope of a_{rp} in Conventional-RBM and TS-RBM (simulation).

The TS-RBM aims to keep a comprehensive index for ride comfort $J_{\text{TS-RBM}}$ at the minimum level, the detailed objective function $J_{\text{TS-RMB}}$ is based on the following Eq.(20), the first item represents the index of vehicle jerk and the latter denotes the PGEP performance in aspect of torsional oscillation. To suppress the vehicle jerk of EV and transient torsional oscillation of PGEP simultaneously, the variables to be designed for TS-RMB in this research include the duration time Δt and coefficients of electric torque curve (c_1, c_2, c_3 and c_4), the optimization result of Δt is 0.09 s.

$$J_{\text{TS - RBM}}(\Delta t, \boldsymbol{x}) = \kappa 1 \cdot \underbrace{\frac{max\left[d\ddot{\theta}_w(t)/dt \Big|_{t=t_0}^{t_0+\Delta t} \right]}{\langle Jerk \rangle_{ref}}}_{\text{vehicle jerk}} + \kappa 2 \cdot \underbrace{\frac{\frac{1}{\Delta t} \cdot \int_{t_0}^{t_0+\Delta t} \left[a_{rp}^2(t) \right] dt}{\langle RMS \rangle_{ref}}}_{\text{torsional oscillation of PGEP}} \tag{20}$$

$$J_{\min} = min\{ J_{\text{TS - RBM}}(\Delta t, \boldsymbol{x}) \} \tag{21}$$

$$\boldsymbol{x} = [c_1, c_2, c_3, c_4] \tag{22}$$

where RMS indicates the root mean square value of a_{rp} during the period of $t_0 \sim t_0 + \Delta t$; *ref* denotes the reference value of vehicle jerk or torsional oscillation by the Conventional-RBM, which is used to normalize the different objective functions; κ_1, κ_2 denote the weighting factors for vehicle jerk and torsional oscillation, and their sum is 1.

Here, in order to obtain a reasonable weighting coefficient (κ_1 and κ_2), sensitivity analysis between the responses of vehicle jerk and torsional oscillation can be concluded from Fig. 22 and Table 2 [45–49]. Four given types of regenerative motor torque curve are designed to test the sensitivity of vehicle jerk and torsional oscillation. As shown in Table 2, the two weighting coefficients reflect the various changing rates between the Conventional-RBM and the TS-RBM, the final values of κ_1 and κ_2 are 0.35 and 0.65 by normalizing the sum of changing rates (1.42 and 0.75), respectively. It should be noted that the above sensitivity analysis is based on the same importance of vehicle jerk and torsional oscillation, in other words, we considered the suppression of vehicle jerk as important as the performance in transmission stability of PGEP.

In this section, a modified genetic algorithm serves to optimize the curve for establishing the electric motor torque during the mode transition process of MD-to-RB. A promising reduction of vehicle jerk and torsional oscillation in EV can be acquired by the TS-RBM proposed in this study based on a detailed genetic algorithm, whose overall framework is depicted in Fig. 23 [50–53].

The optimized curve for motor torque establishment can effectively prevent the vehicle speed from unstable vibration during the

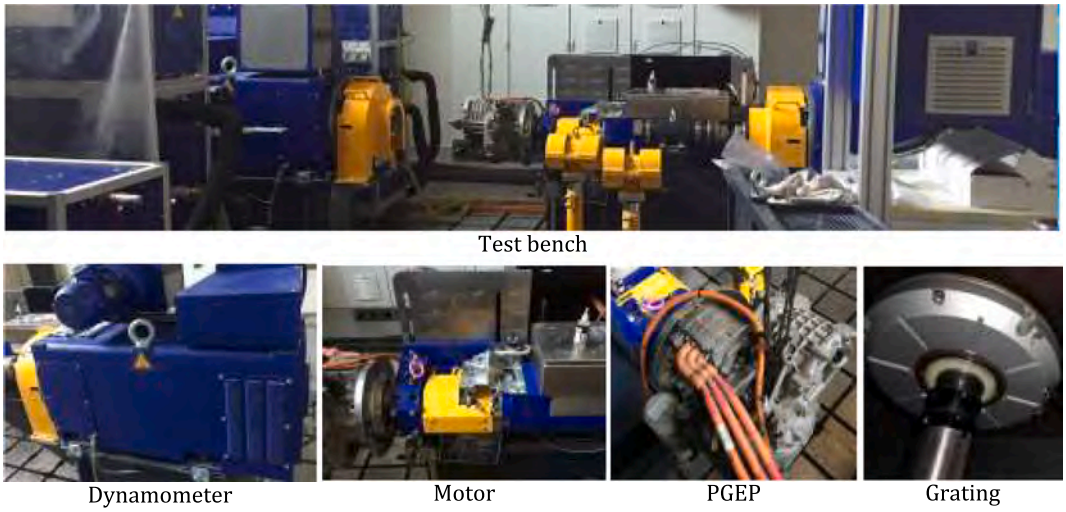

Fig. 27. Schematic graph of the AVL test bench setup.

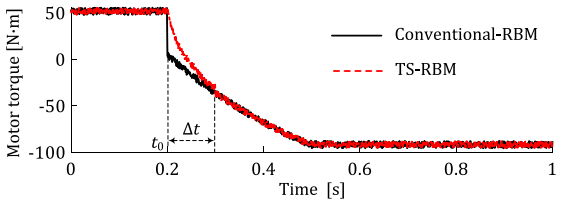

Fig. 28. Real motor torque during MD-to-RB process (experiment).

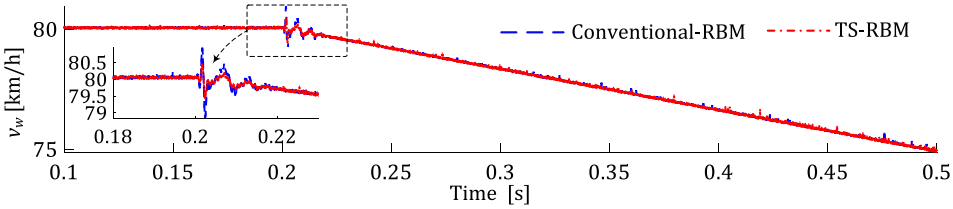

Fig. 29. Dynamic vehicle speed between Conventional-RBM and TS-RBM (experiment).

MD-to-RB mode transition process, the fluctuation amplitude of EV speed in Conventional-RBM and TS-RBM are 2.0 km/h and 0.8 km/h (depicted in Fig. 24). It can be observed that the TS-RBM is able to reduce the amplitude of vehicle speed oscillation by 60% during the MD-to-RB mode transition process.

The comparison of vehicle jerk and PGEP torsional oscillation acceleration with Conventional-RBM and TS-RBM during the MD-to-RB mode transition process is depicted in Fig. 24 and Fig. 25. As can be seen from Fig. 24, TS-RBM is able to reduce the peak value of vehicle jerk from 10.1 m/s^3 to 4.5 m/s^3 after the regenerative braking mode has been triggered at 0.2 s. In the periods of 0.2-to-0.22 s, the RMS values of a_{rp} in Conventional-RBM and TS-RBM are 5.6 m/s^2 and 3.6 m/s^2 (36% down) (See Fig. 26) .

4. Experimental observation and validation of TS-RBM

An AVL test bench is performed as shown in Fig. 27 to verify the transient torsional oscillation-suppression performance of the proposed TS-RBM. The PGEP for experiment is driven by a permanent magnet synchronous motor, which can operate in two states as a driving or a generator motor. And the required hydraulic braking torque is replaced by a terminal load of dynamometer. The whole testing system is mainly composed of electric motor, PGEP transmission, dynamometer, industrial computer, electric control units and battery, which can be charged or discharged by the motor. Torque speed sensor and high accuracy circular grating sensor are employed to get the given input torque and the relative torsional oscillation.

The motor torques including driving torque and regenerative generator torque with Conventional-RBM and TS-RBM are set as the target torques, which will be followed by a PID controller in the PUMA system (Fig. 28), and its corresponding signals are transmitted

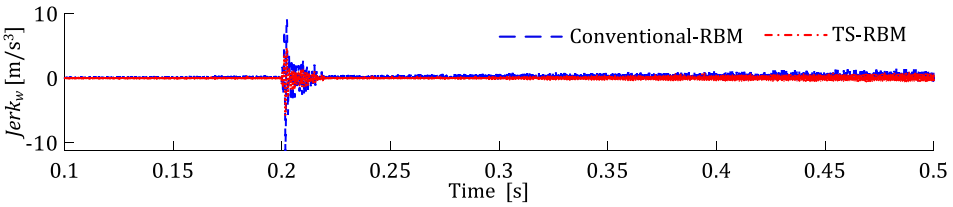

Fig. 30. Vehicle jerk responses of EVs between Conventional-RBM and TS-RBM (experiment).

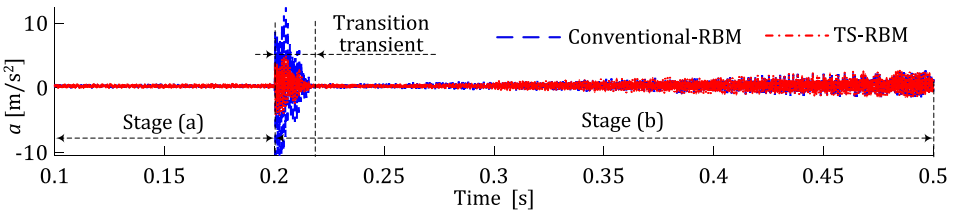

Fig. 31. Transient vibration responses of PGEP between Conventional-RBM and TS-RBM (experiment).

Table 3
Comparison of results between Conventional-RBM and TS-RBM.

Category	Source	Conventional-RBM	TS-RBM	Percentage reduction	Maximum deviation rate
Vehicle jerk of EV	Simulation results	10.1 m/s^3	4.50 m/s^3	55.4%	7.2%
	Experiment results	10.8 m/s^3	4.82 m/s^3	55.3%	
Torsional oscillation of PGEP	Simulation results	5.60 m/s^2	3.60 m/s^2	35.7%	8.7%
	Experiment results	6.04 m/s^2	3.92 m/s^2	35.1%	

through the Controller Area Network (CAN). The vehicle model is simulated by software real-timely in an industrial computer, and the experiment conditions of the performance-test are set as same as the Simulink simulation conditions, and the experiment results are also going to be presented and discussed.

The rig test results shown in Figs. 29–31 are similar with the simulation in previous section. Real-time vehicle speeds in Fig. 29 show that some slightly speed fluctuations appear in a duration of 0.2 ~ 0.22 s, and the maximum speed fluctuations of Conventional-RBM and TS-RBM reach 2.8 km/h and 1.2 km/h comparing with the previous theoretical calculation. The results demonstrate that the oscillations during MD-to-RB transition process of the mathematical model effectively follow the experiment outputs. Although the amplitude of test results is slightly increased due to the inevitable non-stationary excitation of the experimental conditions, TS-RBM also has a better performance than that of Conventional-RBM in aspect of achieving better ride comfort (Fig. 30). Transient torsional oscillation of PGEP (a_{rp}) versus the demanding braking torque is displayed in Fig. 31, the torsional oscillation of PGEP with TS-RBM reduces to nearly one half than that of Conventional-RBM. Therefore, the proposed TS-RBM method is proved to be effective by this studied AVL test bench.).

The vehicle jerk of EV and torsional oscillation of PGEP achieved from simulation and AVL test bench are shown in Table 3, the online simulation results slightly deviate from the experiment results due to uncontrollable error and response delay caused by test equipment. Nevertheless, the maximum discrepancy rate between simulation and experiment is below 8.7%, which comes from unmodelled uncertainties in the dynamical model of the whole system. In conclusion, the established TS-RBM can realizes a more optimal control effect in reducing the torsional oscillation of PGEP and improving the drive comfort of EVs.

5. Conclusion

This paper analyzes the transient torsional oscillation of planetary-gear electrical powertrain during MD-to-RB transition process to improve ride comfort. On the basis of analysis, a novel regenerative braking method for suppression of transient torsional oscillation in planetary-gear electrical powertrain is proposed. The primary vehicle components models, including longitudinal vehicle braking model and transient torsional oscillation model of the planetary-gear electrical powertrain are introduced. According to the theory of braking torque distribution, a method for braking torque distribution which takes account of the braking stability and regeneration of braking energy is proposed to obtain the electric motor torque and external retarding torque during MD-to-RB process. An angle-varying mesh stiffness-considered transmission model and a genetic algorithm-based method for allocation of electric regenerative braking torque are combined to reach a better transient transition performance. The novel torsional oscillation-considered regenerative braking method is evaluated and compared with the Conventional-RBM in simulation and bench test. According to the test results, TS-RBM also has a better performance in aspect of vehicle jerk than Conventional-RBM, thusly achieves a better ride comfort,

Table A1
Nomenclature.

Parameter	Explanation	Parameter	Explanation
oxy	stationary reference frame	c_{sn}	equivalent meshing damping of sun-planet gear
$o_cx_cy_c$	rotary reference frame	c_{rn}	equivalent meshing damping of ring-planet gear
$o_nx_ny_n$	synchronization reference frame	φ_n	included angle
θ_s	dynamic angular displacement of sun gear	z_s	teeth number of sun gear
θ_r	dynamic angular displacement of ring gear	z_r	teeth number of ring gear
θ_{pn}	dynamic angular displacement of planetary gear	z_p	teeth number of planet gear
θ_c	dynamic angular displacement of planetary frame	a_j	j-th fourier expanding coefficients
θ_w	dynamic angular displacement of wheel	Δb_{sn}	1/2 backlashes of sun-planetary gear pair
J_s	inertia of sun gear	Δb_{rn}	1/2 backlashes of ring-planetary gear pair
J_r	inertia of ring gear	i	reduction ratio of PGEP
J_{pn}	inertia of planetary gear	f_r	rolling friction coefficient
J_c	inertia of planetary carrier	C_D	aerodynamic drag coefficient
m_p	mass of planetary gear	A	effective vehicle frontal area
r_{bs}	pitch radii of sun gear	$v(t)$	real-time vehicle speed
r_{br}	pitch radii of ring gear	$a(t)$	real-time vehicle acceleration
r_{bp}	pitch radii of planetary gear	L_F	distance from gravity center to front wheel
r_c	length between center of planet gear and carrier	L_R	distance from gravity center to rear wheel
k_w	torsional stiffness of drive shaft	g	gravity acceleration
c_w	damping of drive shaft	z	braking severity
β	helix angles of helical gear	h_g	height of vehicle gravity center
m	vehicle mass	F_{xF}	longitudinal tire forces of front wheels
δ	equivalent revolving coefficient	F_{xR}	longitudinal tire forces of rear wheels
i_0	final drive ratio	T_{bF_h}	hydraulic braking torque on front wheels
r_w	radius of wheel	T_{bF_m}	electric motor braking torque on front wheels
k_{B1}	equivalent stiffness of wedge brake device	T_{bR_h}	braking torque of the rear wheels
α_s	pressure angles of sun gear	φ	road adhesion coefficient
α_r	pressure angles of ring gear	Δt	duration time
T_m	driving or regenerative torque of electric motor	c_i	electric torque curve coefficients
T_d	external retarding torques	κ_1	weight coefficient of vehicle jerk
k_{sn}	angle-varying mesh stiffness of sun-planet gear	κ_2	weight coefficient of torsional oscillation
k_{rn}	angle-varying mesh stiffness of ring-planet gear	RMS	root mean square value

and the torsional oscillation of PGEP with TS-RBM reduces to nearly one half than that of Conventional-RBM. The test results testify that the established TS-RBM can offer a more optimal control in reducing the torsional oscillation of PGEP and improving the drive comfort of EVs.

In the further, there are three feasible directions for further research of this topic: (1) The performance validation of TS-RBM for other types of electric vehicles; (2) Real vehicle verification with road-surface input disturbance; (3) The performance validation and improvement of the proposed TS-RBM with the incorporation of accurate hydraulic-electric coupled characteristics for powertrain model.

CRediT authorship contribution statement

Feng Wang: Conceptualization, Methodology. **Peng Ye:** Writing - original draft. **Xing Xu:** Supervision. **Yingfeng Cai:** Software, Validation. **Shaoyong Ni:** Investigation. **Hongbo Que:** Writing - review & editing.

Declaration of Competing Interest

The authors declare that they have no known competing financial interests or personal relationships that could have appeared to influence the work reported in this paper.

Acknowledgement

This work is financially supported by the National Natural Science Foundation of China [No. 51705204, U1764257], State Key Laboratory of Engines, Tianjin University [No. K2021-10], Primary Research and Development Plan of Jiangsu Province (CN) [No. BE2019010], Six Talent Peaks Project in Jiangsu Province (CN) [No. JXQC-036], the China Scholarship Council [No. 201908320221], and the China Postdoctoral Science Foundation [No. 2020 M671850].

Appendix

(See Table A1)

References

[1] F. Wang, J. Zhang, X. Xu, Y. Cai, Z. Zhou, X. Sun, A comprehensive dynamic efficiency-enhanced energy management strategy for plug-in hybrid electric vehicles, Appl. Energ. 247 (2019) 657–669.
[2] J. Niu, C. Xu, D. Niu, Comparison on rule based energy management strategy for E-REV, J. Jiangsu U. (Nat. Sci. Ed.) 39 (3) (2018) 266–272.
[3] M.V. Faria, R.A. Varella, G.O. Duarte, T.L. Farias, P.C. Baptista, Engine cold start analysis using naturalistic driving data: city level impacts on local pollutants emissions and energy consumption, Sci. Total. Environ. 630 (2018) 544–559.
[4] G. Fang, L. Tian, M. Fu, M. Sun, R. Du, L. Lu, The effect of energy construction adjustment on the dynamical evolution of energy-saving and emission-reduction system in china, Appl. Energ. 196 (2017) 180–189.
[5] J. Wen, C. Song, Y. Fu, Rotor structure optimization of permanent magnet synchronous generator built in type U, J. Jiangsu U. (Nat. Sci. Ed.) 39 (2) (2018) 194–198.
[6] D. Shi, P. Pisu, L. Chen, S. Wang, R. Wang, Control design and fuel economy investigation of power split hev with energy regeneration of suspension, Appl. Energ. 182 (2016) 576–589.
[7] L. Qiu, L. Wang, Dynamic powertrain design for electric vehicle based on consumption and cost, J. Jiangsu U. (Nat. Sci. Ed.) 40 (1) (2019) 16–21.
[8] X. Zhu, L. Chen, L.i. Quan, Y. Sun, W. Hua, Z. Wang, A new magnetic-planetary-geared permanent magnet brushless machine for hybrid electric vehicle, IEEE T. Magn. 48 (11) (2012) 4642–4645.
[9] J. Ruan, P. Walker, P. Watterson, The dynamic performance and economic benefit of a blended braking system in a multi-speed battery electric vehicle, Appl. Energ. 183 (2016) 1240–1258.
[10] X. Tang, T. Jia, X. Hu, Naturalistic data-driven predictive energy management for plug-in hybrid electric vehicles, IEEE T. Transp. Electr. 7 (2021) 497–508.
[11] J. Ko, S. Ko, Co-operative control for regenerative braking and friction braking to increase energy recovery without wheel lock, Int. J. Auto. Tech-kor. 15 (2014) 253–262.
[12] W. Zhao, G. Wu, Energy transfer and utilization efficiency of regenerative braking with hybrid energy storage system, J. Power Sources. 427 (2019) 174–183.
[13] L. Zhang, X. Cai, Control strategy of regenerative braking system in electric vehicles, Energ. Procedia. 152 (2018) 496–501.
[14] X. Pei, H. Pan, Z. Chen, Coordinated control strategy of electro-hydraulic braking for energy regeneration, Control Eng. Pract. 96 (2020), 104324.
[15] Q. Li, W. Huang, W. Chen, Y.u. Yan, W. Shang, M. Li, Regenerative braking energy recovery strategy based on Pontryagin's minimum principle for fell cell/supercapacitor hybrid locomotive. 44 (11) (2019) 5454–5461.
[16] C. Qiu, G. Wang, New evaluation methodology of regenerative braking contribution to energy efficiency improvement of electric vehicles, Energ. Convers. Manage. 119 (2016) 389–398.
[17] L. Li, X. Li, Analysis of downshift's improvement to energy efficiency of an electric vehicle during regenerative braking, Appl. Energ. 176 (2016) 125–137.
[18] Y. Qin, X. Tang, T. Jia, Z. Duan, J. Zhang, Y. Li, L. Zheng, Noise and vibration suppression in hybrid electric vehicles: state of the art and challenges, Renew. Sust. Energ. Rev. 124 (2020) 109782, https://doi.org/10.1016/j.rser.2020.109782.
[19] Z. Zhang, R. Ma, L. Wang, etc., Novel PMSM control for anti-lock braking considering transmission properties of the electric vehicle, IEEE T. Veh. Technol. 67 (11) (2018) 10378–10386.
[20] J. Liang, D. Paul, Gearshift and brake distribution control for regenerative braking in electric vehicles with dual clutch transmission, Mech. Mach. Theory. 133 (2019) 1–22.
[21] J. Zhang, Y. Li, Time-varying delays compensation algorithm for powertrain active damping of an electrified vehicle equipped with an axle motor during regenerative braking, Mech. Syst. Signal. Pr. 87 (2015) 45–63.
[22] Chen Lv, Junzhi Zhang, Yutong Li, Ye Yuan, Mode-switching-based active control of a powertrain system with non-linear backlash and flexibility for an electric vehicle during regenerative deceleration, P. I. Mech. Eng. D-J Aut. 229 (11) (2015) 1429–1442.
[23] Chen Lv, Junzhi Zhang, Yutong Li, Extended-Kalman-filter-based regenerative and friction blended braking control for electric vehicle equipped with axle motor considering damping and elastic properties of electric powertrain, Vehicle Syst. Dyn. 52 (11) (2014) 1372–1388.
[24] Z. Zhao, J. Chen, Downshift decision and process optimal control of dual clutch transmission for hybrid electric vehicles under rapid braking condition, Mech. Syst. Signal. Pr. 116 (2019) 943–962.
[25] F. Wang, J. Zhang, X. Xu, New method for power allocation of multi-power sources considering speed-up transient vibration of planetary power-split HEV driveline system, Mech. Syst. Signal Process. 128 (C) (2019) 1–18.
[26] S. Wang, J. Li, D. Shi, Control strategy of power-split HEV based on optimal transmission efficiency, J. Jiangsu U. (Nat. Sci. Ed.) 39 (6) (2018) 621–627.
[27] H. Xue, Y. Zhou, Fault diagnosis method for in-wheel motor based on wolf pack algorithm, J. Jiangsu U. (Nat. Sci. Ed.) 40 (15) (2019) 579–584.
[28] F. Wang, J. Xia, X. Xu, New clutch oil-pressure establishing method design of PHEVs during mode transition process for transient torsional vibration suppression of planetary power-split system, Mech. Mach. Theroy. 148 (2020) 1–18.
[29] Y. Tang, L. Wang, R. Zou, Dynamic characteristic of planetary gear transmission system of wind turbine under time-varying speed conditions, J. Jiangsu U. (Nat. Sci. Ed.) 39 (5) (2018) 550–555.
[30] Xiaodong Sun, Yichen Shen, Shaohua Wang, Gang Lei, Zebin Yang, Shouyi Han, Core losses analysis of a novel 16/10 segmented rotor switched reluctance bsg motor for hevs using nonlinear lumped parameter equivalent circuit model, IEEE-ASME T. Mech. 23 (2) (2018) 747–757.
[31] Y. Huangfu, K. Chen, H. Ma, Meshing and dynamic characteristics analysis of spalled gear systems: A theoretical and experimental study, Mech. Syst. Signal Process. 139 (08) (2020) 1–21.
[32] Yifan Huangfu, Zhifang Zhao, Hui Ma, Hongzheng Han, Kangkang Chen, Effects of tooth modifications on the dynamic characteristics of thin-rimmed gears under surface wear, Mech. Mach. Theroy. 150 (2020) 103870, https://doi.org/10.1016/j.mechmachtheory.2020.103870.
[33] S. Gui, Y. Fang, Effect of road roughness coherent function on vehicle-bridge coupling random vibration, J. Jiangsu U. (Nat. Sci. Ed.) 40 (1) (2019) 87–93.
[34] R. He, M. Li, Integrated control strategy of combined braking system and ABS based on road identification, J. Jiangsu U. (Nat. Sci. Ed.) 41 (1) (2020) 20–26.
[35] F. Wang, J. Zhang, X. Xu, New teeth surface and back (TSB) modification method for transient vibration suppression of planetary gear powertrain for an electric vehicle, Mech. Mach. Theroy. 140C (2019) 520–537.
[36] J. Guo, H. Dong, W. Sheng, Optimum control strategy of regenerative braking energy for electric vehicle, J. Jiangsu U. (Nat. Sci. Ed.) 39 (2) (2018) 132–138.
[37] Benjamin Chris Ampimah, Mei Sun, Dun Han, Xueyin Wang, Optimizing sheddable and shiftable residential electricity consumption by incentivized peak and off-peak credit function approach, Appl. Energ. 210 (2018) 1299–1309.
[38] F. Wang, X. Xu, Z. Fang, L. Chen, Study of the influence mechanism of pitch deviation on cylindrical helical gear meshing stiffness and vibration noise, Adv. Mech. Eng. 9 (9) (2017) 1–9.
[39] C. Liu, Z.D. Fang, F. Wang, An improved model for dynamic analysis of a double-helical gear reduction unit by hybrid user-defined elements: Experimental and numerical validation, Mech. Mach. Theory 127 (9) (2018) 96–111.
[40] J. Yang, F. Gong, H. Zhang, Tooth profile modification and tooth contact analysis of precision forging spiral bevel gear, J. Jiangsu U. (Nat. Sci. Ed.) 39 (2) (2018) 168–173.
[41] Ren He, Xiang Tian, Yunlei Ni, Yiqiang Xu, Mode transition coordination control for parallel hybrid electric vehicle based on switched system, Adv. Mech. Eng. 9 (8) (2017), https://doi.org/10.1177/1687814017715564.
[42] X. Zhu, H. Zhang, B. Yang, G. Zhang, X. Zhu, H. Zhang, Cloud-based shaft torque estimation for electric vehicle equipped with integrated motor-transmission system, Mech. Syst. Signal Process. 99 (2018) 647–660.
[43] Y. Li, H. Wu, Frontier techniques and prospect of in-wheel motor for electric vehicle, J. Jiangsu U. (Nat. Sci. Ed.) 40 (3) (2019) 261–268.
[44] Liang Li, Xiangyu Wang, Rui Xiong, Kai He, Xujian Li, AMT downshifting strategy design of HEV during regenerative braking process for energy conservation, Appl. Energ. 183 (2016) 914–925.
[45] E. Zhou, X. Zhu, J. Lu, Flow deformation analysis of post liquefaction sand based on VOF method, J. Jiangsu U. (Nat. Sci. Ed.) 39 (4) (2018) 485–491.

[46] Fangwei Xie, Xudong Zheng, Yaowen Tong, Bing Zhang, Xinjian Guo, Dengshuai Wang, Yun Wang, Effect of two phase flow on transmission torque of oil film at high rotational speeds, Ind. Lubr. Tribol. 70 (8) (2018) 1367–1373.
[47] J. Qu, C. Wang, X. Li, H. Wang, Heat transfer performance of flexible oscillating heat pipes for electric/ hybrid-electric vehicle battery thermal management, Appl. Therm. Eng. 135 (5) (2018) 1–9.
[48] W. Tao, Z. Liu, Seat suspension control of wheel loader based on damping state switching, J. Jiangsu U. (Nat. Sci. Ed.) 40 (5) (2019) 504–510.
[49] Mohammed Takase, Ting Zhao, Min Zhang, Yao Chen, Hongyang Liu, Liuqing Yang, Xiangyang Wu, An expatiate review of neem, jatropha, rubber and karanja as multipurpose non-edible biodiesel resources and comparison of their fuel, engine and emission properties, Renew. Sust. Eenerg. Rev. 43 (2015) 495–520.
[50] F. Wang, X. Xu, Z. Fang, L. Chen, Design and analysis of herringbone gear with sixth-order transmission error based on meshing vibration optimization, Adv. Mech. Eng. 9 (6) (2017) 1–12.
[51] T. Wang, F. Liu, Y. Gao, N. Hu, Precise scheduling of Beidou agricultural machinery based on combination of genetic algorithm and WiFi clustering algorithm, J. Jiangsu U. (Nat. Sci. Ed.) 41 (4) (2020) 426–433.
[52] X. Zhu, Z. Xiang, L. Quan, Y. Chen, L. Mo, Multi-mode optimization research on a multi-port magnetic planetary gear permanent magnet machine for hybrid electric vehicles, IEEE T. Ind. Electron. 12 (5) (2018) 1–10.
[53] Hao Liu, Shunyi Shi, Ping Yang, Jianming Yang, An improved genetic algorithm approach on mechanism kinematic structure enumeration with intelligent manufacturing, J. Intell. Robot. Syst. 89 (3-4) (2018) 343–350.